ATOMIC OXYGEN STUDIES ON POLYMERS

W. D. Morison, R. C. Tennyson, J. B. French, T. Braithwaite
University of Toronto, Institute for Aerospace Studies

M. Moisan and J. Hubert
Université de Montréal

ABSTRACT

The purpose of this research investigation was to study the effects of atomic oxygen on the erosion of polymer based materials. This report describes the development of an atomic oxygen 'neutral' beam facility using a 'SURFATRON' surface wave launcher that can produce beam energies between 2 and 3 eV at flux levels as high as $\sim 10^{17}$ atoms/cm^2-sec. Thin film dielectric materials were studied to determine recession rates and reaction efficiencies (R_e) as a function of incident beam energy and fluence. Accelerated testing was also demonstrated and the values of R_e compared to available space flight data. In addition, SEM photomicrographs of the samples' surface morphology were compared to flight test specimens.

INTRODUCTION

The space environment is characterized by the presence of charged particles, various atomic species (in low concentrations), "vacuum", micrometeoroids, radiation, temperature extremes and man-made debris. To some degree, all of these factors influence the design of satellites, depending upon the orbital altitude. Of particular concern is the presence of atomic oxygen, the concentration of which is shown in figure 1 (ref. 1) along with other atomic species and charged particles. The operation of many satellites, the Space Shuttle and the future U.S. Space Station, in low earth orbit (LEO), presents a major design problem since it is well established that atomic oxygen seriously erodes many of the commonly employed spacecraft materials (see ref. 2, for example). Although the concentration values shown in figure 1 may appear to be insignificant compared to the particle concentration at the earth's surface ($\sim 10^{19}$/cm^3), the actual flux of atoms impinging on an orbiting vehicle is quite high because of the satellite orbital velocity of ~8 km/sec (corresponding to an incident atomic oxygen energy of ~5 eV. Figure 2 (ref. 3) presents a plot of the incident flux as a function of altitude and solar activity. For reference purposes, the space shuttle altitude is indicated, corresponding to a flux of between $10^{14} \sim 10^{15}$ (atoms/cm^2-sec).

To qualify materials for spacecraft applications, it is necessary to assess

*Financial support for this research was provided by the Auburn University Space Power Institute, Subcontract No. 86-207, issued under their Prime Contract No. N60921-86-C-A226 with the U.S. Naval Surface Weapons Center (Dalgren, Va.) and the Ontario Centre for Advanced Materials under Grant No. TP2-325.

their sensitivity to atomic oxygen, as measured by their reaction efficiency (R_e) at orbital conditions. This is defined to be the volume of material lost per incident oxygen atom. Up to this point in time, limited flight test data at LEO conditions is available (see ref. 4). Consequently, it is imperative that ground-based systems be developed that can accurately simulate the neutral atomic oxygen environment in LEO. Such a system is described in this report together with comparative test data on mass loss rates, reaction efficiencies and surface morphology changes. Many of the materials tested in this simulator are compared to flight test data to ascertain the "validity" of the simulation. It will also be demonstrated that "accelerated testing" is possible, in that it yields erosion results consistent with flight data.

UTIAS ATOMIC OXYGEN (AO) BEAM FACILITY

A schematic of the UTIAS AO facility configuration is presented in figure 3. This system is comprised of three major components (see photographs, fig. 4): a microwave induced plasma torch, a sampler-skimmer interface, and a vacuum chamber with the associated support electronics. The plasma torch is used to generate a stream of essentially neutral oxygen atoms seeded in a helium gas carrier. The sampler-skimmer system strips off a portion of the lighter carrier gas from the plasma and produces a diverging AO beam which is then directed into the connecting vacuum chamber. The chamber, in the form of a glass 'cross', maintains candidate AO bombardment samples at approximately 10^{-5} torr, to approximate low earth orbit spacecraft surface conditions.

SURFACE WAVE LAUNCHER (SURFATRON)

There are various ways of producing plasmas with microwave (>300 MHz) power. The device used at UTIAS (fig. 5) is referred to as a 'SURFATRON' because it operates by propagating an electromagnetic surface wave along the plasma column. With such a device, a wave is excited at a given location along a cylindrical vessel containing the gas to be ionized. Providing the wave power flow is large enough, as this wave propagates, its energy is used to sustain the plasma column. It is called a surface wave because most of the power flows axially, very close to the surface of the dielectric vessel that contains the plasma column. This situation corresponds to the wave field decreasing radially, away from the plasma column, in an exponential-like fashion.

The surface wave is a natural propagation mode (an eigen-mode) along a plasma column. The efficient transformation of the microwave power into the plasma is a consequence of the use of this mode.

There are essentially two distinct elements in the SURFATRON surface wave launcher: the launching gap — a small interstice of circular symmetry through which the electric field leaks out toward the plasma — and an impedance matching system. In terms of an equivalent circuit, the gap can be represented by a capacitance and a resistance, and the impedance matching part is generally equivalent to two LC circuits (ref. 5). When properly designed and tuned, the two circuit components cancel out any imaginary component at the launcher input part and permit impedance matching of the launcher-plasma assembly and the transmission line. This ensures optimum power transfer from the generator (ref. 6).

PLASMA CHARACTERISTICS

The microwave generated, atmospheric pressure helium plasma has been studied and characterized in terms of excitation temperature, gas temperature and electron density (ref. 7).

The SURFATRON is normally operated with a metered 98.5% helium/1.5% oxygen gas supply and is powered by a 200 Watt, 2450 MHz Microtron microwave power supply. The plasma is located in a 2 mm ID × 4 mm OD alumina (AL23) discharge tube. The power is set at 195 W and the total input flow rate is maintained at 3ℓ/min. Under these conditions, the excitation temperature is on the order of 2800 K, the degree of dissociation of O_2, as determined by mass spectrometer measurements, is approximately 64 percent, and the fraction of oxygen in the excited state is less than 1.2 percent (ref. 8).

SAMPLER-SKIMMER SYSTEM

The helium/oxygen plasma is discharged at atmospheric pressure and allowed to expand supersonically toward the sampler-skimmer system. This system (fig. 6) consists of two nickel sampling/skimming orifice cones which are separated by an evacuated, water-cooled interface chamber. As the plasma discharge impinges upon the sampler cone, a portion of the central plasma core is drawn into the interface. Further, rapid expansion of the discharge takes place in the interface toward the skimmer core. A fraction of one percent of the flow through the sampler is stripped out by the skimmer cone and passed into the test chamber. The skimmer throughput is a largely mono-energetic, slightly divergent beam of helium, atomic oxygen and molecular oxygen, with a mean free path in excess of 1 metre. The interface pressure and the sampler-skimmer geometry govern the rate of molecular flow through the skimmer and consequently, the pressure in the test chamber and the atomic oxygen flux at the target.

Over a period of time, erosion of the sampler cone was observed, as manifested by an increase in interface pressure. An extensive series of measurements of the increase in orifice diameter (D_{sa}) were made as a function of system time. The results of these tests are given in figure 7. This data was necessary to permit accurate calculations of the atomic oxygen flux, as detailed in the Appendix.

TORCH ALIGNMENT

Clearly, the key to conducting a successful experiment is the ability to produce repeatable results. Results from early operation of the facility suggested some difficulty associated with the alignment of the torch and the sampler-skimmer interface.

The optimum system alignment should maximize the amount of atomic oxygen in the beam. Since slight misalignment of the system leads to entrainment of room air into the chamber, an alternate approach is simply to minimize the amount of room air being entrained. Since room air is the system's only source of nitrogen, this is easily accomplished by tuning the mass spectrometer to the N_2^+ peak, and adjusting the SURFATRON's position until the peak height is minimized. The N_2^+ peak minimization method proved viable, as AO damage to samples became consistently better correlated. It was then realized that the total chamber pressure would also

be minimized along with the partial pressure of the nitrogen. This fact allowed a more precise alignment, as the Bayard-Alpert gauge is much "smoother" and easier to read than the mass spectrometer. When coupled to a digital voltmeter, the Bayard-Alpert gauge permitted the system to be aligned to a fine tolerance. Subsequent tests demonstrated that this alignment procedure reduced scatter to approximately 4% (ref. 9).

VACUUM SYSTEM AND ELECTRONICS

The test chamber, a 15 cm diameter × 25 cm diameter 'Visiflow' glass cross (figs. 3, 4), incorporates fixtures to hold both control and test samples, Bayard-Alpert and Penning type gauges for pressure measurement, and an Aerovac AVA-1 mass spectrometer for beam analysis. An Edwards 250/200M 'Diffstak' pump extracts gas from the chamber at a rate of 2300 ℓ/s to produce system pressures on the order of 10^{-5} torr.

A time-of-flight chopper system is currently being installed for beam energy surveys. These features allow complete monitoring of changes in beam properties such as atomic oxygen flux, energy, average molar mass, and degree of oxygen dissociation, as the system gas flow and geometry parameters are varied.

CHARACTERISTICS OF THE ATOMIC OXYGEN BEAM

The enclosed Appendix contains a detailed gas flow analysis for the AO facility.

BEAM ENERGY

From equation (18) (Appendix), it is clear that for a given molar mass of gas, measurements of the plasma temperature will define the peak oxygen atom energy. Since nozzle beam systems produce beams with relatively narrow velocity distributions (ref. 10), the peak energy will correspond closely to the average value.

Figure 8 shows plots of beam energy (E) versus molar mix (M_{mix}) for various plasma temperatures. As the constituents of the gaseous mixture ($He/O_2/Ar$) are varied, corrections to the plasma temperature must be made. The resulting "adjusted" experimental curve is shown in figure 8.

Because the beam is diverging slightly from the sampler-skimmer interface, intermolecular collisions in the test chamber are very infrequent. As a result, the energy distribution within the beam should remain undisturbed, except for a broadening associated with the beam divergence and the corresponding reduction in the atomic oxygen flux.

ATOMIC OXYGEN FLUX

From the Appendix, the atomic oxygen flux at some distance x_i is given by equation (13), i.e.,

$$\Phi_{AO} = \frac{3.45\times10^{18}}{(10.65 + x_i)^2} \quad \text{(atoms/cm}^2\text{-sec)}$$

for $x_i \geq 7.86$ cm.

For the positions defined by $3.93 \leq x_i \leq 7.86$ cm, the significant beam blocking effect of the sample produces multiple atomic oxygen strikes and enhances the effective flux such that

$$\Phi_{AO} = \frac{1.695\times10^{27}}{(10.65 + x_i)^{8.86}} \qquad 3.93 \leq x_i < 7.86 \text{ cm}$$

This phenomenon produces highly accelerated erosion rates for samples in this region. Figure 9 depicts the flux variation described by the above functions and shows the relative testing 'acceleration factor', based upon the ratio of the simulator flux to the nominal atomic oxygen flux in low earth orbit (250 km, $\approx 3\times10^{14}$ atoms/cm^2-s). Figure 9 clearly shows that acceleration factors, nominally in the range 3 to 275, are achievable with the present facility configuration.

BEAM EROSION PROFILE

The variation in flux across the beam diameter was assessed initially by profiling exposed samples using a Sloan Technology Corporation DEKTAK 3030 surface profile measuring system. This device uses a diamond tipped stylus to scan the surface of a sample in 2000 steps, with a vertical resolution of 20 μm. Figure 10 shows a plot from the DEKTAK. Because of the irregular surface profiles, it is difficult to obtain an accurate measurement of the volume of material eroded.

RECESSION RATE PROFILE

One parameter used to assess the erosion effects of atomic oxygen is the recession rate (R_r), which is a measure of the depth of material removed per unit time (cm/s). When a thin film is completely eroded, the recession rate is known exactly at the edge of the hole, and is given by,

$$R_r = h/t$$

where h = thickness of film (cm) and t = exposure time (s). If a series of identical films is exposed to the same beam for varying periods of time, a recession rate profile can be produced. The plot of R_r versus hole radius should not only give the recession rate distribution, but should also depict the beam profile in terms of the cross-sectional variation in flux. Figure 11 shows recession rate versus hole radius for a 2.29×10^{-3} cm (0.9 mil) Kapton®-H film. The profile has been extended out to r = ~1.0 cm although examination of the samples suggests that the maximum effective beam radius is approximately 0.575 cm. Note that, except for vertical scaling, the profile of figure 11 is consistent with the profilimeter results in figure 10.

EXPERIMENTAL RESULTS

SENSITIVITY TO BEAM ENERGY

A set of experiments was undertaken to determine if the reaction efficiency was dependent upon the incident AO beam energy. Because of the present upper limit on energy for the UTIAS AO simulator, it was necessary to demonstrate that material mass loss rates comparable to those obtained in space flight tests could be achieved.

From equation (18) (Appendix), it is shown that the beam energy can be controlled by changing the molar mass (M_{mix}) of the gas mixture and the plasma temperature. For the UTIAS system, the temperature change that occurs with varying M_{mix} is given in figure 8. By varying the concentration of the gas mixture ($He/O_2/Ar$) it was possible to obtain a sensitivity curve of reaction efficiency as a function of beam energy for Kapton, as shown in figure 12. Note that reaction efficiency for Kapton can be calculated from equation (16) (Appendix) once the mass loss rate is determined. It is quite apparent that a threshold exists for Kapton reaction efficiency near 1.5 eV. For comparison purposes, the space flight value (ref. 2) of 3×10^{-24} cm^3/atom is plotted at 5 eV. Similar results were also obtained for Mylar.

SENSITIVITY TO BEAM FLUX

Tests were conducted on Kapton-H film using a 2.2 eV atomic oxygen beam for different flux levels. The mass loss versus exposure time curves are presented in figure 13. It can be seen that at the higher flux values ($\geq 10^{16}$ atoms/cm^2-sec) there is a transition region in which the material mass loss rate response changes. This is particularly evident for the curve at 10^{16} atoms/cm^2-sec. It was found that beyond this transition region, at flux levels $\leq 10^{16}$ atoms/cm^2-sec, the mass loss rates approached a constant. For Kapton-H film, $\Delta m/\Delta t \approx 0.075$ (mg/sec). Substituting this value into equation (16) (Appendix) yields a reaction efficiency for Kapton of $R_e \simeq 2.99\times10^{-24}$ (cm^3/atom).

SEM photomicrographs of the Kapton samples' surface morphology are presented in figure 14, for different exposure times, at a flux of $\Phi \simeq 8.3\times10^{16}$ (atoms/cm^2-sec). It is quite apparent that the surface characteristics are changing with fluence. This is particularly evident when one compares photos (a) and (b) in the transition region discussed above.

ACCELERATED TESTING

One of the major applications of ground-based simulators is the potential to do accelerated testing. Clearly, the validity of such a procedure rests on the assumption that for constant fluence tests ($F = \Phi \times$ time), the same material reaction efficiency will be obtained. Experiments were conducted with Kapton-H film, at different flux levels, at exposure times beyond the transition range. Two test samples, (A) and (B), are compared (see figure 13) in the following table:

Sample*	Beam Area (cm^2)	Φ (atoms/cm^2 s)	t (s)	F (atoms/cm^2 s)	$\Delta m/\Delta t$ (mg/s)	R_e (cm^3/atom)
A	1.995	8.3×10^{16}	2,700	2.24×10^{20}	$.395\times10^{-3}$	3.06×10^{-24}
B	1.765	10^{16}	21,600	2.16×10^{20}	$.075\times10^{-3}$	2.99×10^{-24}

*ρ = 1.42 (gm/cm^3)

It can be seen that the same value of R_e is obtained, providing the tests are conducted at fluences beyond the transition range. Furthermore, comparing photomicrographs for samples (A) (figure 14(b)) and (B) (figure 15), shows a remarkable match in surface morphology. Thus it seems reasonable to assume that accelerated testing is valid for assessing material sensitivity to atomic oxygen.

MATERIAL REACTION EFFICIENCY

Using the procedures previously described, a series of tests were conducted on the materials listed in table 1. Comparisons with LEO flight data reported in reference 2 are also included. Note that the results have been "normalized" to Kapton as a reference material. To convert the data to R_e values, assume R_e(Kapton) $\simeq 2.99\times10^{-24}$ (atoms/cm^2-sec). In general the results are in reasonable agreement with flight data. However, it should be noted that some uncertainty exists in the flight data because of errors in estimating the incident flux.

Figure 16 presents some SEM photomicrographs for several of the thin-film materials. These results provide a further basis for comparison with flight samples for given fluences.

CONCLUSIONS

An AO beam facililty has been developed based on a microwave powered SURFATRON device that can produce AO energies up to 2.2 eV, at flux levels as high as 8×10^{16} (atoms/cm^2-sec). This system operates continuously and can yield target diameters up to 4.9 cm.

Reaction efficiencies (R_e) have been measured for a variety of materials and good correlation with LEO flight data has been obtained. It has been demonstrated that accelerated testing can be employed to yield the same value of R_e for a given fluence. SEM photomicrographs exhibit "identical" surface morphology for the accelerated test comparisons. Other notable observations include an energy threshold that must be achieved to obtain values of R_e consistent with flight tests, and that a start-up transition region exists at certain flux levels in which material mass loss rates differ from longer term exposure values.

REFERENCES

1. Van der Waal, P. C.: Effect of Space Environment on Materials. Royal Netherlands Aircraft Factories Fokker, Rept. RV-22, 1968.

2. Leger, L.; Visentine, J.; and Santos-Mason, B.: Selected Materials Issues Associated with Space Station. Proc. 18th International SAMPE Technical Conference, Oct. 1986.

3. Peplinski, D. R.: Satellite Exposure to Atomic Oxygen in Low Earth Orbit. NASA CP 2340, 1984.

4. Leger, L.; Santos-Mason, B.; Visentine, J; and Kuminecz, J.: Review of LEO Flight Experiments. Proc. NASA Workshop on Atomic Oxygen. Nov. 1986, JPL Pub. No. 87-14, June 1987.

5. Moisan, M.; Zakrzewski, Z.; and Pantel, R.: The Theory and Characteristics of an Efficient Surface Wave Launcher (Surfatron) Producing Long Plasma Columns. J. Phys. D: Appl. Phys., Vol. 12, 1979.

6. Moisan, M.; Ferreira, C. M.; Hajlaoui, Y.; Henry, D.; Hubert, J.; Pantel, R.; Ricard, A.; and Zakrzewski, Z.: Properties and Applications of Surface Wave Produced Plasmas. Rev. Physique Appliquée, Vol. 17, 1982, pp. 707-727.

7. Besner, A.; Moisan, M.; and Hubert, J.: Fundamental Properties of Radiofrequency and Microwave Surface-Wave Induced Plasmas. J. Anal. Atom. Spectrosc., to be published Sept. 1988.

8. Lam, Calvin K.: Development of a Nozzle Beam Containing Atomic Oxygen. University of Toronto Institute for Aerospace Studies, UTIAS Tech. Note No. 153, July 1970.

9. Braithwaite, T. H.: Development of an Atomic Oxygen Beam Facility for Low Earth Orbit Simulation. M.A.Sc. Thesis, University of Toronto Institute for Aerospace Studies, 1988.

10. Knuth, Eldon L.; and Kuluva, Neil M.: Performance of an Arc-Heated Supersonic Molecular Beam and Its Application to Molecule-Molecule Collision Studies. Rec. Adv. in Aerothermochemistry, Vol. 1, NATO AGARD, Paris, 1967.

TABLE 1 - MATERIAL REACTION EFFICIENCY (R_e) COMPARISON WITH LEO FLIGHT DATA (REF. 2)

Material	LEO Flight Data		AO Simulator
	R_e (cm^3/atom)	$R_e/(R_e)_{Kapton}$	$R_e/(R_e)_{Kapton}$
Kapton-H	3×10^{-24}	1	1
Polyethylene	3.7	1.23	0.987
Mylar	3.4	1.13	1.360
Tedlar	3.2	1.07	1.260
Pyrolytic Graphite	—	—	0.318
HOPG*	—	—	0.478
Carbon	0.9~1.7	0.30~0.57	—
Teflon FEP	<0.05	<0.017	0.019

*Highly Oriented Pyrolized Graphite

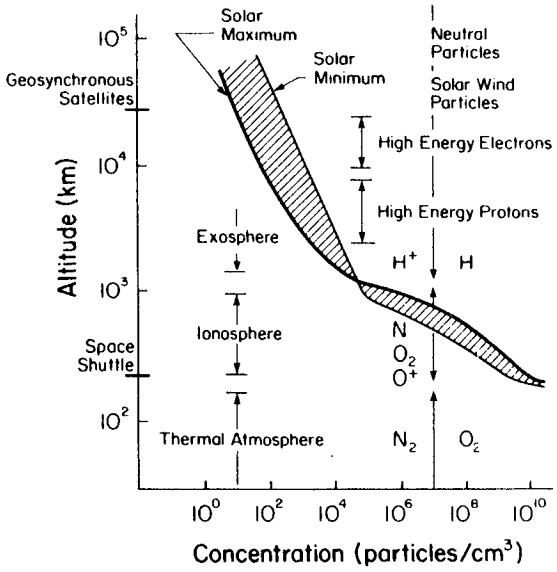

Fig. 1 (from Ref. 1)

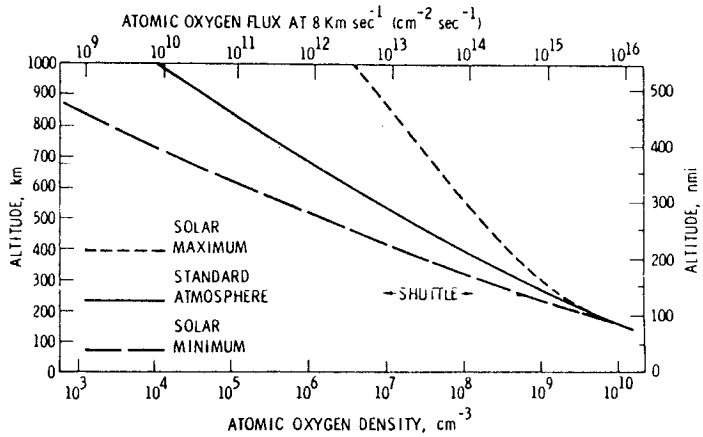

Fig. 2 (from Ref. 3)

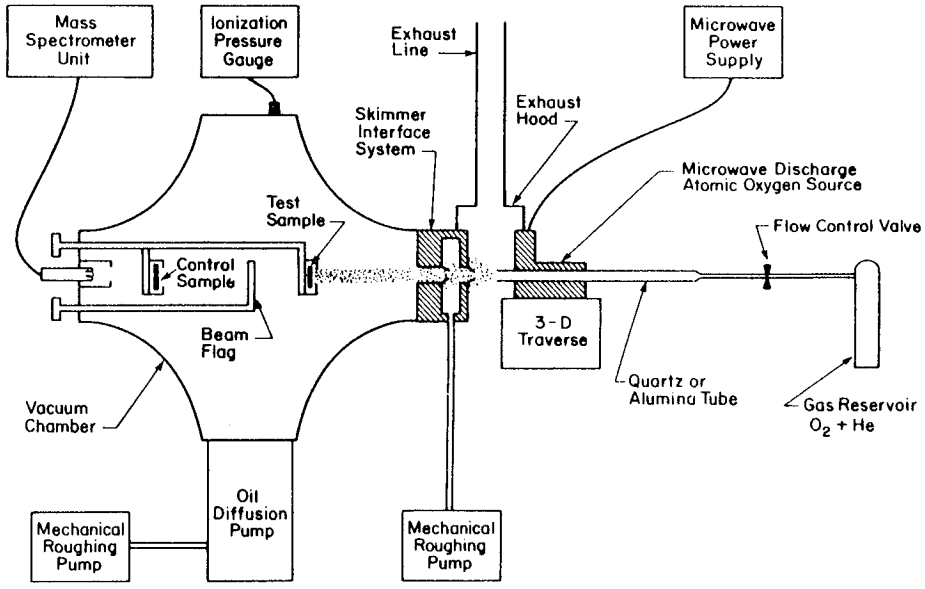

Fig. 3 Schematic of UTIAS Atomic Oxygen Beam Facility

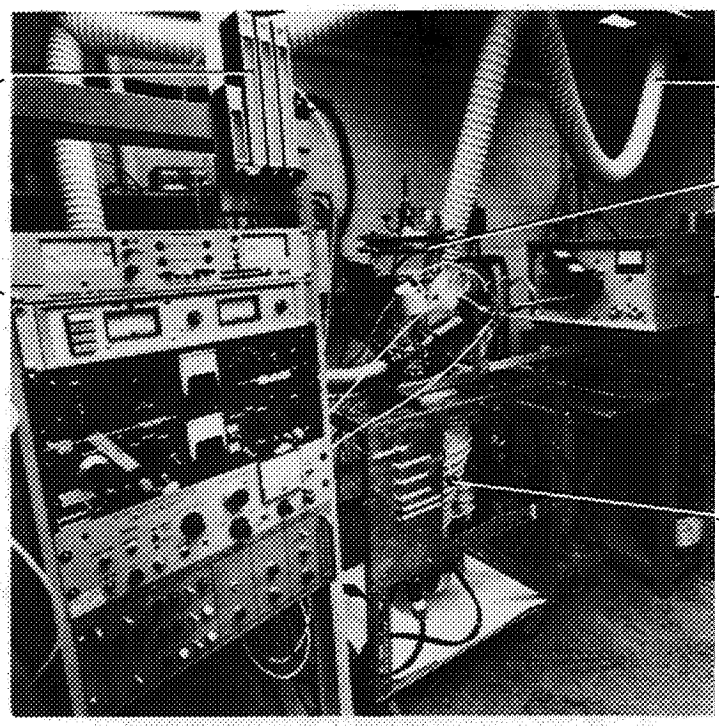

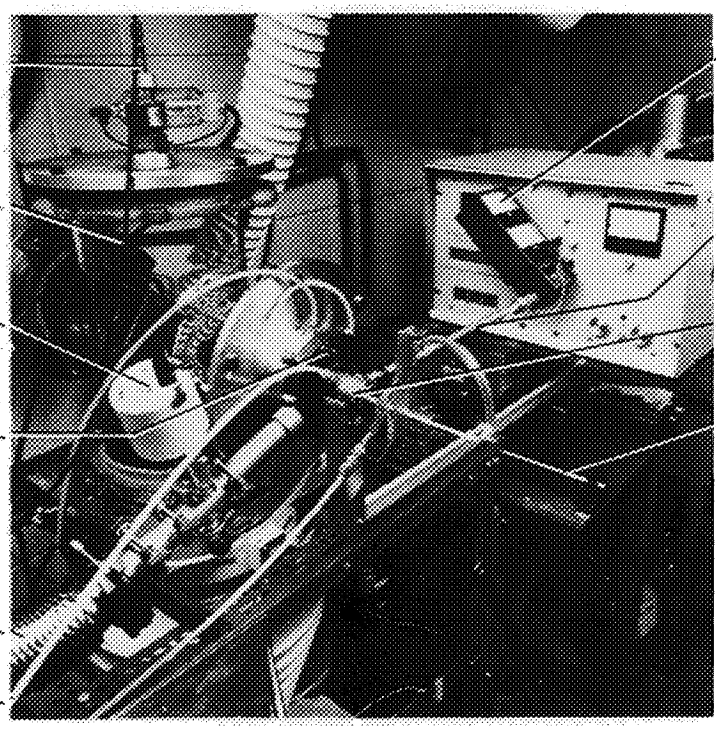

Fig. 4 The UTIAS Atomic Oxygen Beam Facility

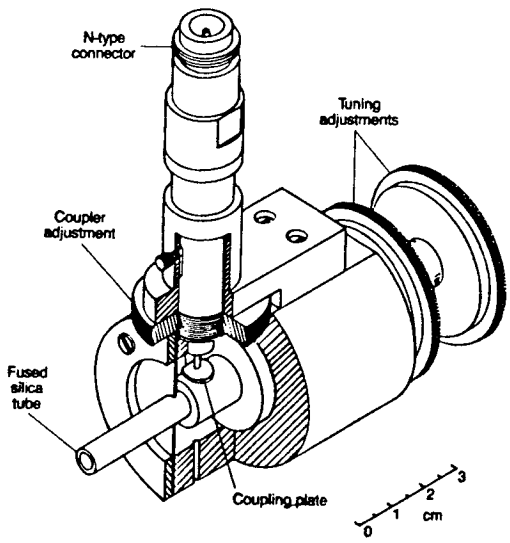

Fig. 5 Surfatron - a Microwave Surface Wave Launcher
(from Ref. 3)

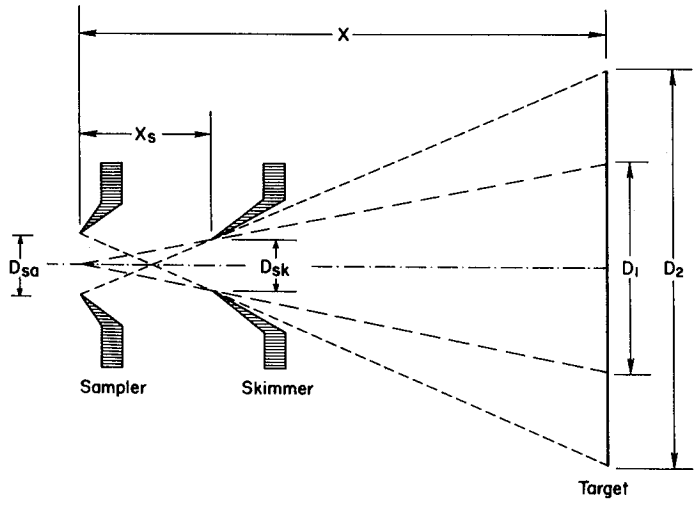

Fig. 6 Sampler Skimmer Geometry

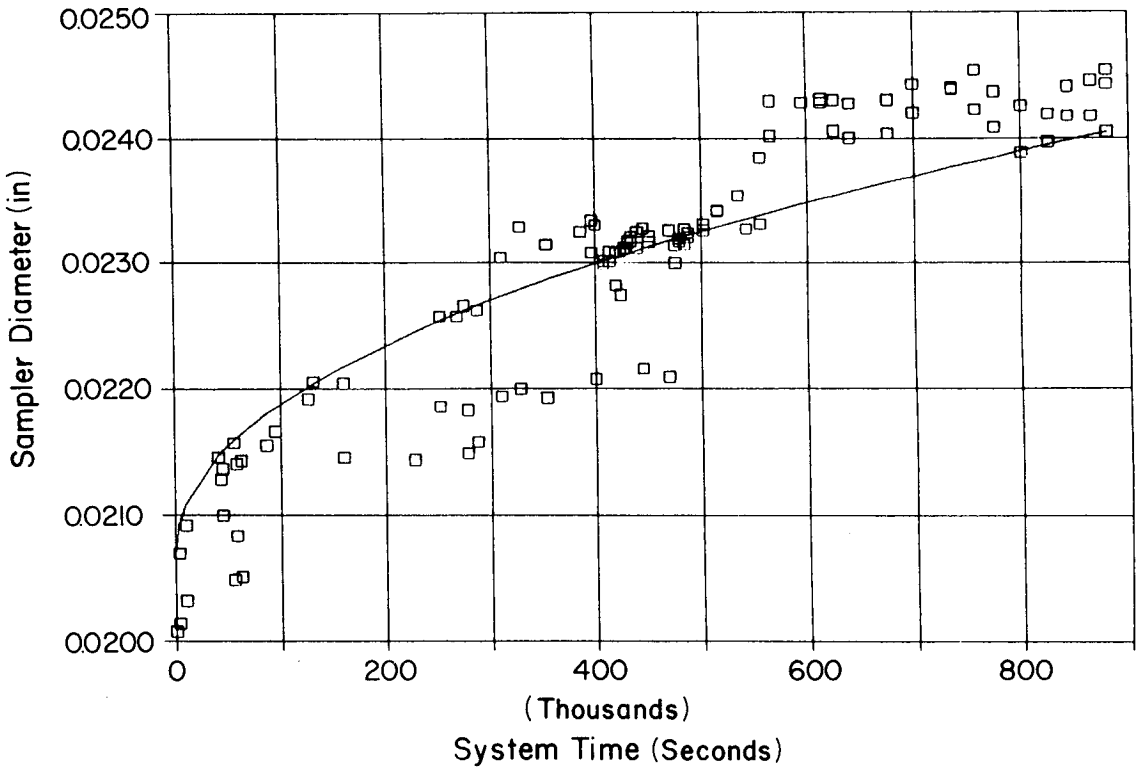

Fig. 7 ORIFICE DIAMETER vs SYSTEM TIME
Sampler #2 Initially .0207"

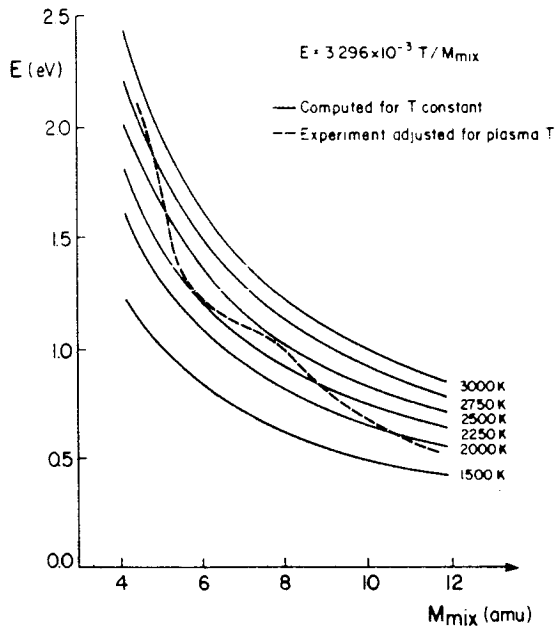

Fig. 8 Beam Energy as a Function of Gas Mixture

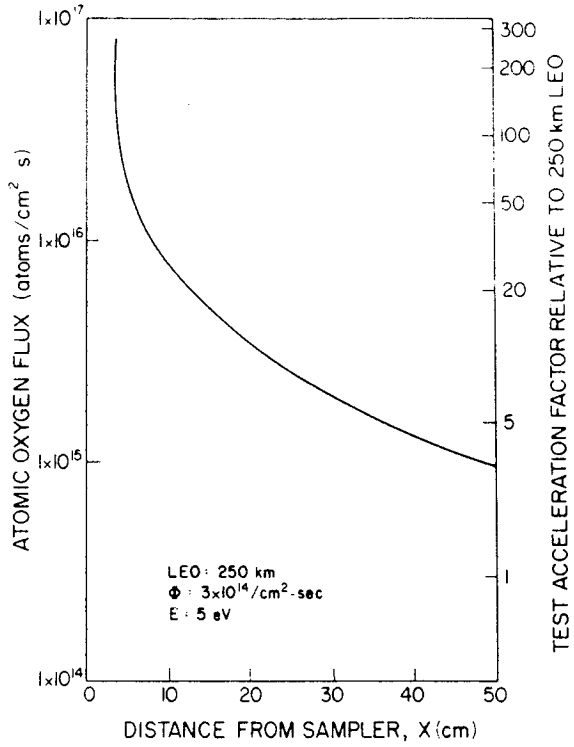

Fig. 9 Atomic Oxygen Flux and Accelaration Factor vs Distance from Sampler Orifice

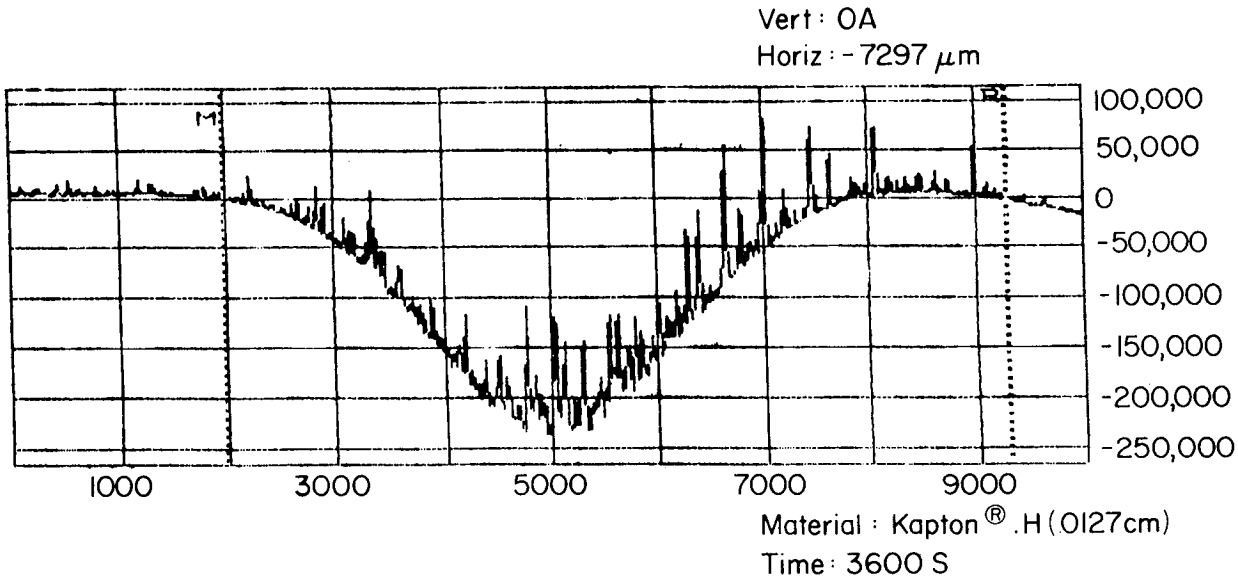

Fig. 10 AO beam profile using DEKTAK Profilimeter

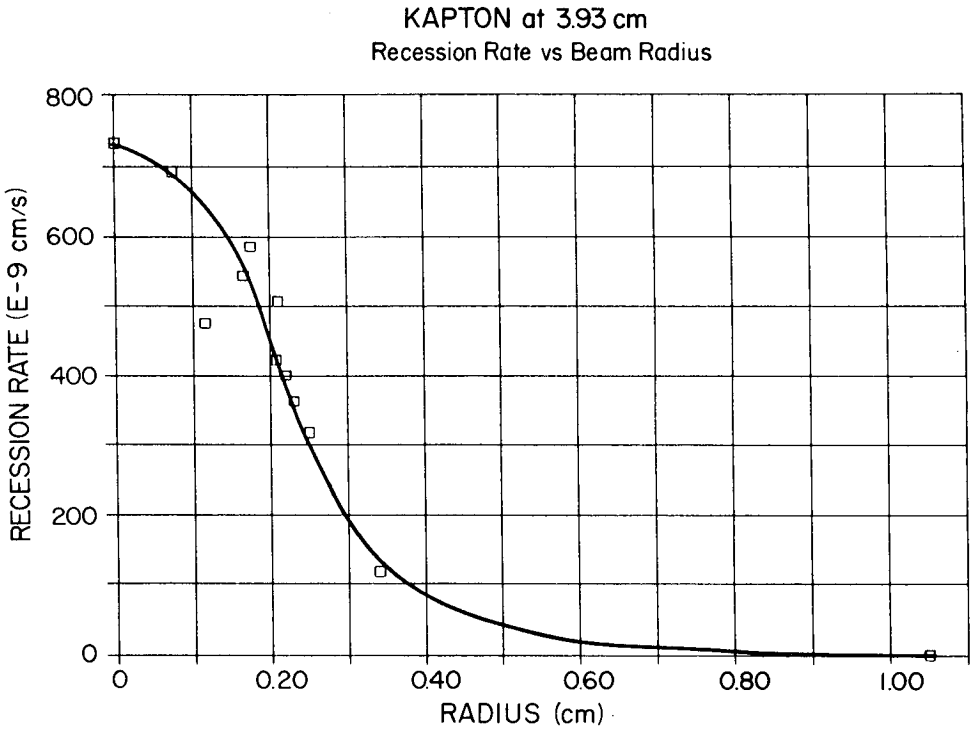

Fig. II AO beam profile using hole radii

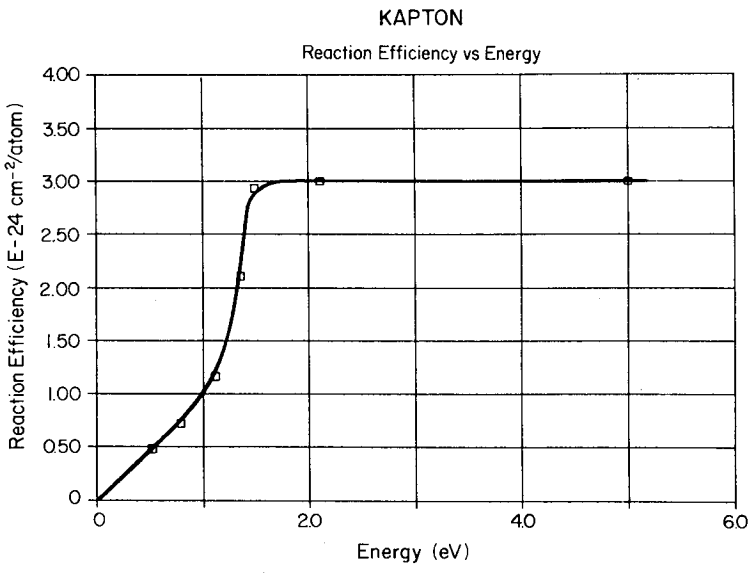

Fig. 12

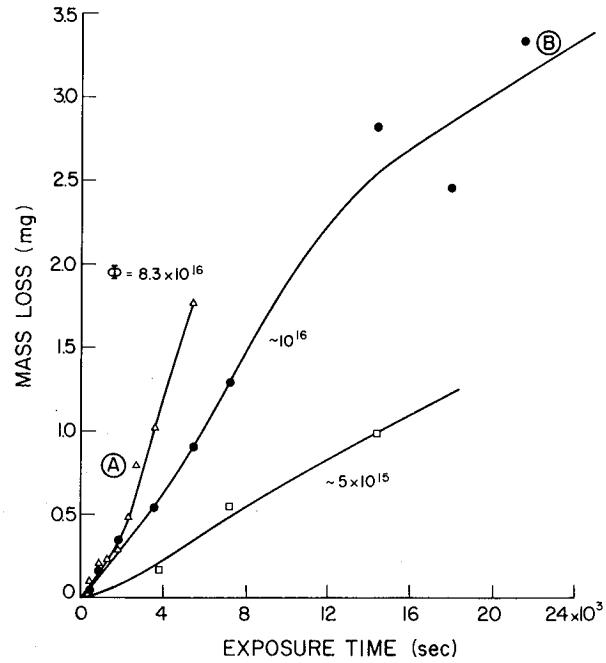

Fig. 13 Effect of Atomic Oxygen Flux on the Erosion Rate of KAPTON-H in UTIAS AO Beam Facility

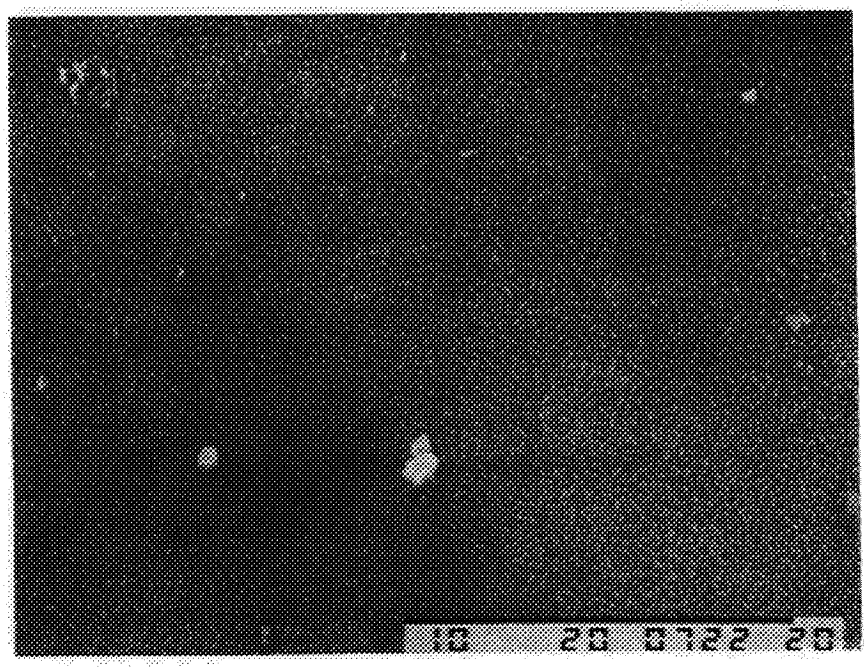

a) $t = 240\ s,\ F \simeq 2 \times 10^{19}\ (atoms/cm^2)$

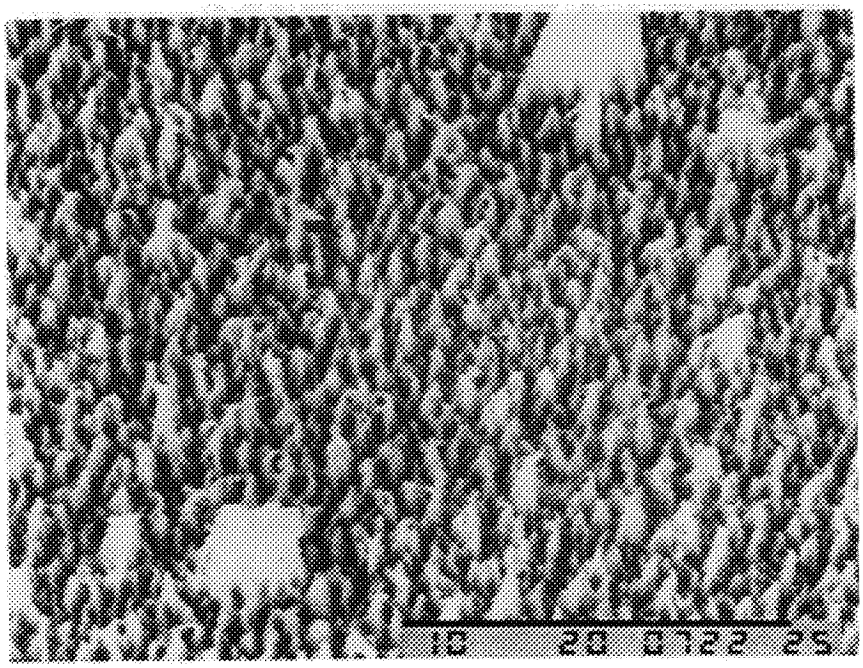

b) $t = 2700\ s,\ F \simeq 2.24 \times 10^{20}\ (atoms/cm^2)$

Fig. 14 SEM Photomicrographs of Kapton® -H Film at 5000X, 7° tilt, $\Phi \simeq 8.3 \times 10^{16}$ (atoms/cm^2-s)

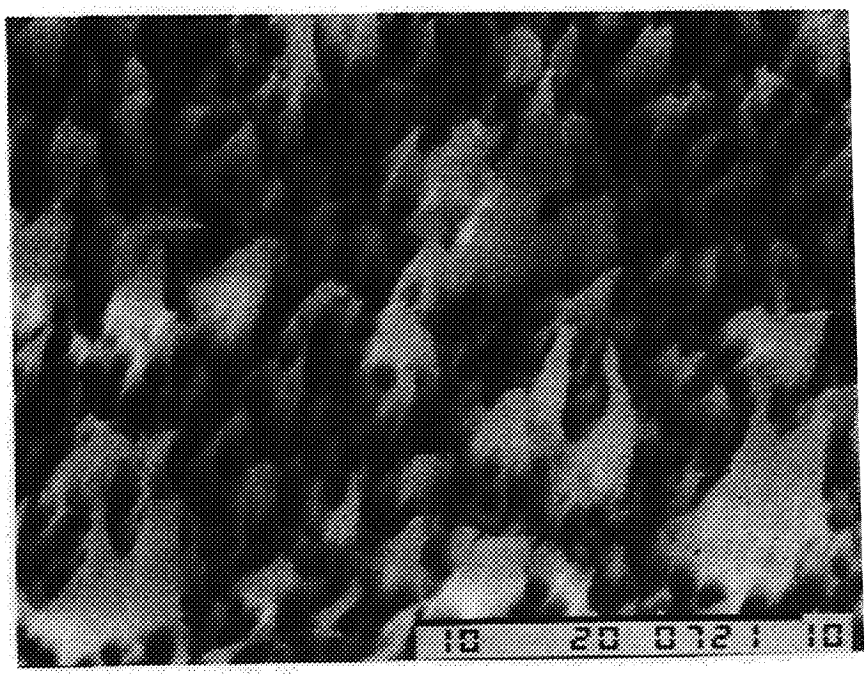

c) $t = 5400\,s$, $F \simeq 4.48 \times 10^{20}$ (atoms/cm^2)

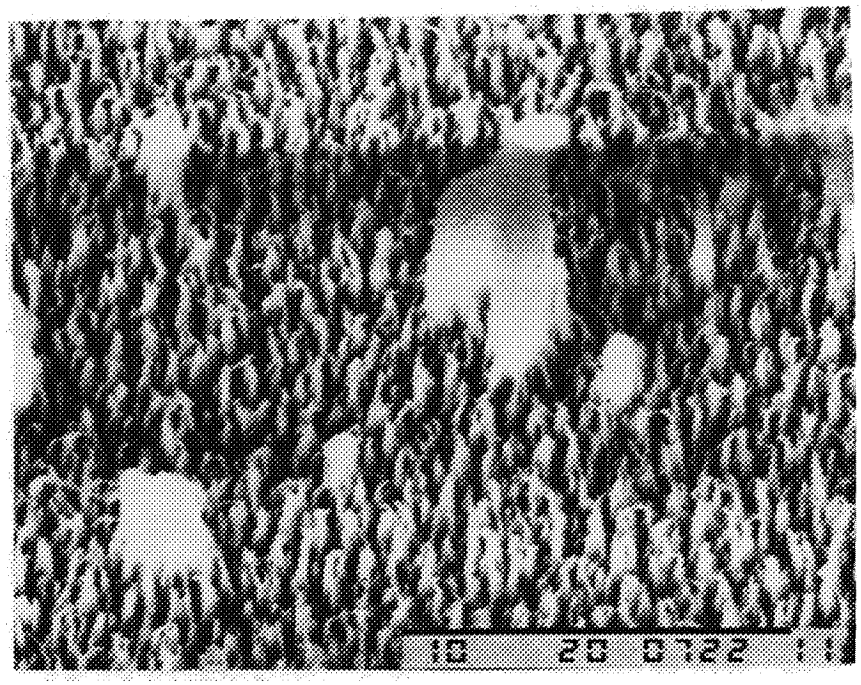

d) $\Phi \simeq 10^{16}$ (atoms/cm^2-s), $t = 21{,}600\,s$,
$F \simeq 2.16 \times 10^{20}$ (atoms/cm^2)

Fig. 15 SEM Photomicrographs of Kapton® -H Film at 5000X, 7° tilt

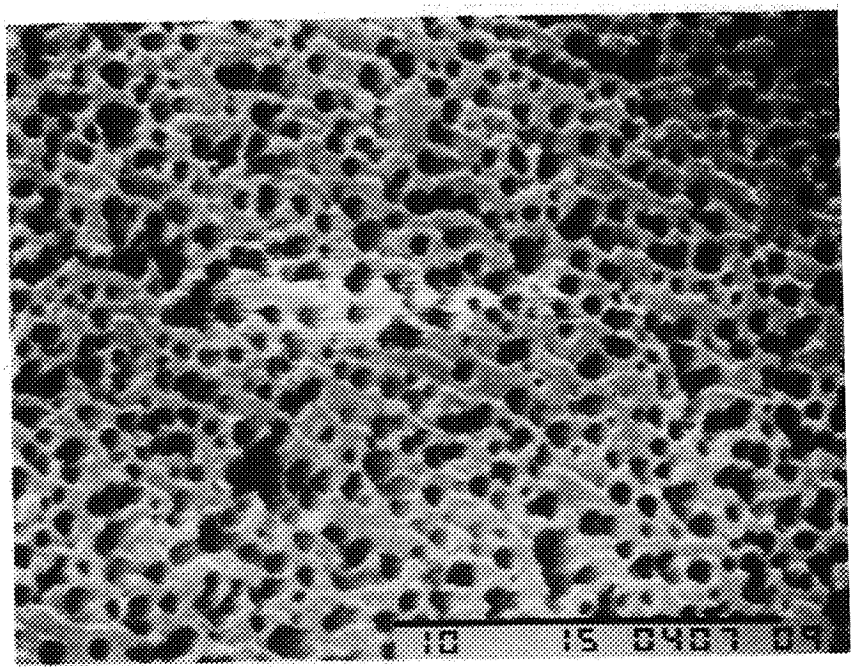

Polyethylene : $\Phi \simeq 5.6 \times 10^{15}$ (atoms / cm^2-s)

$F \simeq 3.4 \times 10^{20}$ (atoms / cm^2)

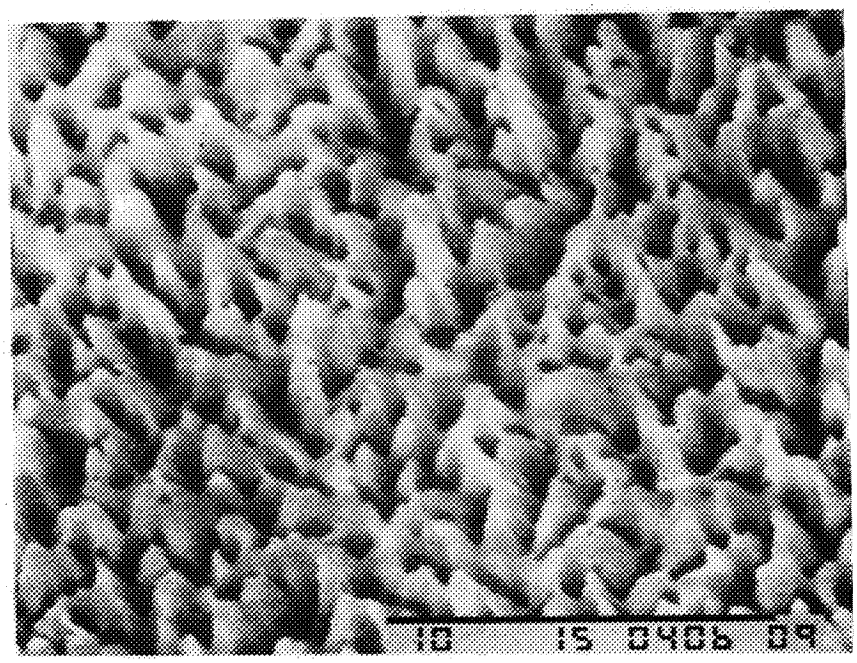

TEFLON FEP : $\Phi \simeq 3 \times 10^{16}$ (atoms / cm^2-s)

$F \simeq 1.4 \times 10^{21}$ (atoms / cm^2)

Fig. 16 SEM Photomicrographs at 5000X, 7° tilt

APPENDIX - GAS FLOW ANALYSIS FOR AO BEAM FACILITY

It has been shown (refs. 8, 9) that the gas flow rate through the sampler orifice is described by

$$G_{sa} = n^*a^*A^* = \left(\frac{2}{\gamma+1}\right)^{\frac{1}{2}\left(\frac{\gamma+1}{\gamma-1}\right)} \cdot n_o a_o A_o \quad \text{(molecules/sec)} \tag{1}$$

where $\gamma \simeq 1.62$, n_o = molecular density at orifice (molecules/cm^3), a_o = speed of sound (cm/s), and A^* = orifice area (cm^2). Since

$$a_o = 11.736 \times 10^3 \sqrt{T/M} \quad \text{(cm/s)} \tag{2}$$

where T = absolute gas temperature (K), M = average molar mass (amu), and

$$n_o = n \frac{T_{ref}}{T} = \frac{7.339 \times 10^{21}}{T} \quad \text{(molecules/sec)} \tag{3}$$

where n = Lochschmidt number = 2.687×10^{19} atoms/cm^2, and T_{ref} = 273.16 K.

Also $A = \frac{\pi}{4} D_{sa}^2$, D_{sa} = orifice diameter

so that

$$G_{sa} = 3.833 \times 10^{25} \frac{D_{sa}^3}{\sqrt{TM}} \tag{4}$$

If the flow into the chamber through the skimmer orifice is neglected, the pressure in the interface can be determined from

$$G_{sa} = 3.24 \times 10^{19} P_x S_x \text{ (atoms/sec)} \quad \text{where } P_x = \text{interface pressure (torr)}, \; S_x = \text{pump speed } (\ell/\text{sec}) \tag{5}$$

For nozzle beam systems (refs. 8, 9), the flow through the skimmer orifice and into the test chamber is given by

$$G_{sk} = 0.631 \, G_s \Omega, \quad \text{where } \Omega = \text{solid angle subtended by skimmer orifice} = A_{sk}/x_s^2 \tag{6}$$

and $A_{sk} = \frac{\pi D_{sk}^2}{4}$, D_{sk} = skimmer orifice diameter = 0.04826 cm; x_s = sampler skimmer spacing = 0.754 cm (7)

so that $G_{sa} = 1.231 \times 10^{21}$ molecules/sec and $G_{sk} = 2.498 \times 10^{19}$ molecules/sec. The flow of oxygen atoms in the chamber is given by

$$G_{AO} = \left(\frac{2\alpha}{1+\alpha}\right)\beta \cdot G_{sk},$$ where α = degree of dissociation of O_2; β = fraction of plasma-source O_2 in beam

The degree of dissociation is determined from mass spectrometer measurements of the beam. Analysis of the relative change in oxygen peak heights, originally presented by Lam (ref. 8), was modified to include a correction for room air entrained by the plasma. Mass spectrometer data are also used to quantify the change in gas stream composition that results from room air entrainment. The parameter β expresses the amount of plasma-source oxygen in the beam relative to the total molecular flow through the skimmer orifice.

For the sampler-skimmer geometry defined above, and for a 0.985 He/0.015 O_2 plasma, the mass spectrometer data yields: $\alpha = 0.632$ and $\beta = 0.0092$ so that $G_{AO} = 1.78 \times 10^{16}$ (AO/sec). An average volumetric erosion rate can be determined from mass loss measurements on a sample, following exposure to the atomic oxygen beam, as

$$\dot{V} = \Delta m/t\rho \quad (cm^3/s) \tag{9}$$

where Δm = mass loss (g), t = exposure time (s), and ρ = specific gravity (g/cm^3). The reaction efficiency (R_e) for the material can then be determined from G_{AO} and $\dot{V}$ as

$$R_e = \frac{\dot{V}}{G_{AO}} \quad (cm^3/atom) \tag{10}$$

Alternatively, the material reaction efficiency may be determined from G_{AO} and a study of beam diameter as a function of distance from the sampler orifice:

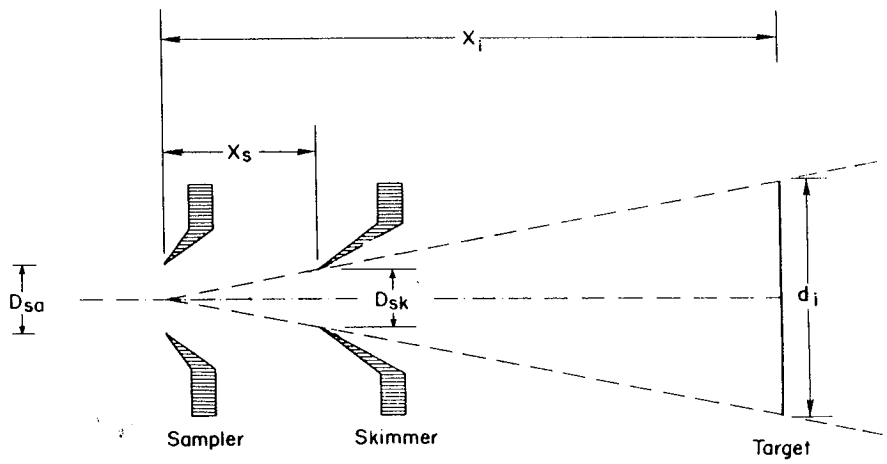

If A_t = target area (beam area) = $\pi d_i^2/4$ at a distance x_i, it has been found that the system yields the following expression for target beam diameter

$$d_i = 0.081\ (10.65 + x_i) \tag{11}$$

and so

$$A_t = 5.15\times10^{-3}\ (10.65 + x_i)^2,\ x_i \geq 7.86\ \text{cm} \tag{12}$$

Then the atomic oxygen flux at the target is

$$\Phi_{AO} = \frac{G_{AO}}{A_t} = \frac{3.45\times10^{18}}{(10.65 + x_i)^2}\ (\text{atoms/cm}^2\text{-s})\ \text{for}\ x_i \geq 7.86\ \text{cm} \tag{13}$$

The atomic oxygen fluence (F) is computed simply from the flux and the exposure time as

$$F = \Phi_{AO} \cdot t = \frac{3.45\times10^{18}\,t}{(10.65 + x_i)^2}\ (\text{atoms/cm}^2) \tag{14}$$

The material recession rate (R_r) is determined from the volumetric erosion rate $\dot{V}$ by

$$R_r = \frac{\dot{V}}{A_t} = \frac{194.06\ \dot{V}}{(10.65 + x_i)^2}\ (\text{cm/s}) \tag{15}$$

The material reaction efficiency can be computed in an equivalent fashion as

$$R_e = \frac{R_r}{\Phi_{AO}} = 5.62\times10^{-17}\ \frac{\Delta m}{\rho t} \tag{16}$$

The average energy of the oxygen atoms can be evaluated from

$$E = \frac{5}{2}\,kT\,\frac{M_{O_1}}{M_{mix}} \tag{17}$$

where k = Boltzmann constant $\equiv 8.24\times10^{-5}$ (eV/K), T = average plasma temperature (K), M_{O_1} = oxygen atom molar mass = 16 amu, M_{mix} = average molar mass of plasma input gas so that

$$E = 3.296 \times 10^{-3} \frac{T}{M_{mix}} \quad (eV) \tag{18}$$

The value of M_{mix} is fixed by the input gas stream (and slightly altered by the influence of the dissociated oxygen), so that a valid measure of the plasma temperature yields the oxygen atom energy directly.

In practice, the expression shown below and in figure 14 is used to determine the plasma temperature:

$$TM_{mix} = 1.40 \times 10^{12} \frac{D_{sa}^4}{P_x^2 S_x^2} \tag{19}$$